Revista de la Academia Colombiana de Ciencias Exactas, Físicas y Naturales. 2026
doi: https://doi.org/10.18257/raccefyn.3273

Physical Sciences

Original article

Experimental Deconvolution of Electronic and Thermal Switching Mechanisms in the VO_2 Metal-Insulator Transition

Deconvolución Experimental de los Mecanismos de Conmutación Electrónicos y Térmicos en la Transición Metal-Aislante del VO_2

Juan Gabriel Ramírez

Department of Physics, Universidad de los Andes, Bogotá, Colombia

Inaugural article as a Correspondent Member of the Academia Colombiana de Ciencias Exactas, Físicas y Naturales

Abstract

The metal-insulator transition (MIT) in vanadium dioxide (VO_2) represents a canonical correlated electron system where electronic correlations and structural distortions operate cooperatively. We present an experimental methodology to deconvolute electronic and thermal switching pathways using temperature-dependent pulsed current-voltage measurements that minimize self-heating effects. The switching landscape decomposes into electronic branches (weak temperature dependence and thermal branches (parabolic dependence, Joule heating). The identified electronic branches enable applications in neuromorphic memories and high-frequency oscillators. This work provides direct experimental evidence for simultaneous operation of both mechanisms, establishing a quantitative framework for voltage-driven phase transitions in correlated oxides.

Keywords: Metal-insulator transition; Vanadium dioxide; Strongly correlated systems.

Resumen

La transición metal-aislante (MIT) en el dióxido de vanadio (VO_2) representa un sistema canónico de electrones correlacionados donde correlaciones electrónicas y distorsiones estructurales operan cooperativamente. Presentamos una metodología experimental para deconvolucionar las vías de conmutación electrónica y térmica mediante mediciones pulsadas corriente-voltaje dependientes de temperatura, minimizando efectos de auto-calentamiento. El espectro de conmutación se descompone en ramas electrónicas (débil dependencia térmica y ramas térmicas (dependencia parabólica, calentamiento Joule). Las ramas electrónicas identificadas permiten aplicaciones en memorias neuromórficas y osciladores de alta frecuencia. Este trabajo proporciona evidencia experimental directa de la operación simultánea de ambos mecanismos, estableciendo un marco cuantitativo para transiciones de fase impulsadas por voltaje en óxidos correlacionados.

Palabras clave: Transición metal-aislante; Dióxido de vanadio; Sistemas fuertemente correlacionados.

Introduction

The metal-insulator transition in vanadium dioxide has evolved from a contentious ”Mott versus Peierls” debate into sophisticated understanding of orbital-selective hybrid mechanisms where electron correlations and structural distortions operate cooperatively (**Kim, Kang, Mun, *et al.,*** 2022; **Pouget, Launois, D'Haenens, Merenda, & Rice,** 1975; **Tomczak & Biermann,** 2012). Modern theoretical and experimental work has established that VO_2 undergoes a correlation-assisted Peierls transition, where a_{1g} orbitals exhibit a correlation-enhanced Peierls transition while e^{π}_{g} orbitals undergo a Mott transition with orbital ordering (**Kim *et al.,*** 2022). This orbital selectivity explains why previous single-

Citation: Ramírez JG. Experimental Deconvolution of Electronic and Thermal Switching Mechanisms in the VO_2 Metal-Insulator Transition. Revista de la Academia Colombiana de Ciencias Exactas, Físicas y Naturales. 2026 Ene 30. doi: https://doi.org/10.18257/raccefyn.3273

Editor: Edgar Emir González

Corresponding autor:
Juan Gabriel Ramírez;
jgramirez@uniandes.edu.co

Received: August 7, 2025
Accepted: October 14, 2025
Published on line: January 30, 2026

Revista de la Academia Colombiana de Ciencias Exactas, Físicas y Naturales. 2026
doi: https://doi.org/10.18257/raccefyn.3273

mechanism theories failed to capture the full complexity of the transition and highlights the intrinsically coupled nature of electronic and structural degrees of freedom (**Wall et al.**, 2018; **Sood et al.**, 2021).

In electrically-driven devices, these fundamental mechanisms manifest as distinct switching pathways that have proven challenging to separate experimentally. Electronic mechanisms are characterized by weak temperature dependence and dominate when electric fields directly modify orbital occupancy or trigger carrier injection effects, typically manifesting at ultrafast timescales (sub-nanosecond) (**O'Callahan et al.**, 2015; **Markov, Appavoo, Haglund, & Sil**, 2015; **Morrison et al.**, 2014). Thermal mechanisms exhibit strong temperature dependence and become prominent through Joule heating effects, particularly at longer timescales and in steady-state operation where power dissipation drives local heating (**Murtagh et al.**, 2020; **Zimmers et al.**, 2013; **Li et al.**, 2016). The central challenge has been to experimentally deconvolute these contributions during device operation, as both mechanisms can produce similar macroscopic switching behavior despite their fundamentally different physical origins.

Systematic studies comparing different vanadium oxides have revealed that the relative contribution of electronic versus thermal mechanisms depends critically on material resistivity, device geometry, and thermal coupling to the environment (**Valmianski et al.**, 2018). In nanoscale devices, thermal effects become suppressed due to enhanced thermal coupling, allowing purely electronic contributions to emerge more prominently. Recent work has further clarified this picture by showing that the switching mechanism can cross over from purely thermal to non-thermal depending on the sample's defect density, with field-assisted carrier generation from defect states enabling the non-thermal pathway (**Kalcheim et al.**, 2020). However, beyond extrinsic defect-mediated processes, intrinsic field effects may also arise directly from the Mott component of the MIT itself. These intrinsic mechanisms involve field-induced band modification and orbital occupancy changes that can trigger the transition independent of defect-mediated processes, reflecting the fundamental correlation-driven nature of the electronic switching pathway that becomes accessible when thermal contributions are minimized.

Understanding this interplay is crucial not only for fundamental physics but also for technological applications. Smart windows exploit electronic mechanisms for rapid optical switching (**Yang et al.**, 2019), while memory devices utilize thermal mechanisms for stable state retention (**Zhou & Ramanathan**, 2016). The ability to control and separate these mechanisms opens pathways for engineering devices with tailored responses, from ultrafast switches to adaptive memory elements for neuromorphic computing architectures (**del Valle, Ramírez, Rozenberg, & Schuller**, 2018).

Previous studies have identified signatures of both thermal and electronic contributions (**Valmianski et al.**, 2018; **Rathi et al.**, 2015; **Pósa et al.**, 2023), but a clear experimental method to separate and map their respective influences has been lacking. Theoretical work suggests that resistance changes spanning 4-5 orders of magnitude result from the interplay of both mechanisms, with switching requiring current densities of 10^3-10^6 A/cm^2 and threshold voltages of 1-3 V for microscale devices (**Kumar et al.**, 2014).

Here, we introduce a comprehensive experimental methodology that uses temperature-dependent pulsed current-voltage measurements to deconvolute and characterize the coexisting thermal and electronic switching mechanisms in VO_2 devices. We demonstrate that the complex switching landscape can be decomposed into distinct branches, each with unique temperature dependence revealing its physical origin. Our results provide direct experimental validation for the cooperative nature of the MIT and establish a quantitative framework for understanding electrically-driven phase transitions in correlated oxides.

Methods

Device Fabrication

Vanadium oxide thin films (90 nm thick) were prepared by reactive RF magnetron sputtering of a vanadium target onto r-cut sapphire substrates. The deposition was performed in a high vacuum system (base pressure $< 5\times10^{-8}$ Torr) with an Ar/O_2 gas mixture at a total pressure of 3×10^{-3} Torr and an oxygen partial pressure of 1.5×10^{-4} Torr. The substrate was held at 500°C during deposition. These films were verified to be single-phase VO_2 via X-ray diffraction, exhibiting the characteristic MIT around 340 K (**Sharoni et al.,** 2008).

Microscale two-terminal devices were fabricated using standard e-beam lithography and lift-off techniques. Metallic electrodes consisting of a 50 nm vanadium adhesion layer and a 100 nm gold layer were deposited by sputtering. This process defined devices with channel lengths ranging from sub-micron to 10 μm. The final device geometry was defined by etching the surrounding VO_2 in argon plasma, leaving an isolated square of VO_2 under the electrodes.

Electrical Characterization

Current-voltage (I-V) characteristics were measured using a pulsed current-reversal method to minimize self-heating during data acquisition, enabling clearer distinction of non-thermal effects. For each device, comprehensive I-V curves were recorded at numerous stabilized ambient temperatures (T_a), close to 200, spanning from below to well above the intrinsic T_{MIT} of VO_2. Pulse measurements were performed to characterize the volatile switching dynamics, with particular attention to the temporal evolution that reveals the interplay between electronic and thermal mechanisms (**Kumar et al.**, 2014; **Joushaghani et al.**, 2014).

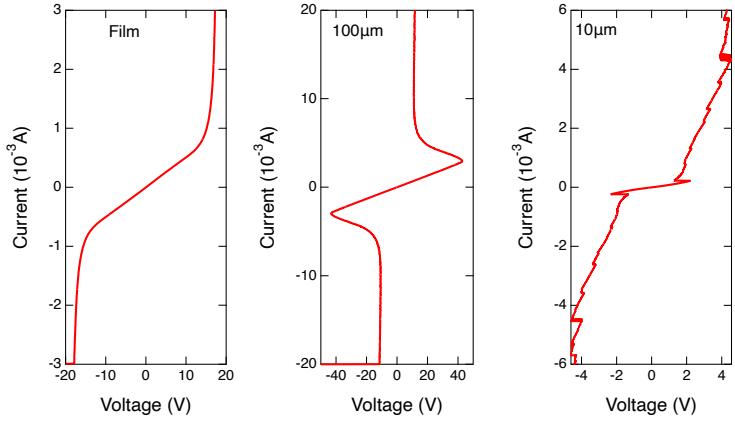

Figure 1. Scale-dependent evolution of current-voltage characteristics in VO_2 devices at room temperature. I-V measurements at T = 300K showing the transition from bulk to discrete switching behavior: (a) macroscopic sample (film) displaying smooth, continuous MIT characteristic of ensemble behavior; (b) 100 μm device exhibiting negative differential resistance (NDR) indicating transition region; (c) 10 μm device showing discrete voltage jumps that reveal individual switching mechanisms on top of NDR.

Results

Scale-Dependent Emergence of Discrete Switching Events

We first examine how geometric confinement affects the manifestation of different switching mechanisms. Figure 1 shows I-V measurements at room temperature for devices of

Revista de la Academia Colombiana de Ciencias Exactas, Físicas y Naturales. 2026
doi: https://doi.org/10.18257/raccefyn.3273

varying sizes. The macroscopic sample (Fig. 1a) exhibits smooth, continuous behavior consistent with ensemble averaging over multiple domains (**Ramírez, Sharoni, Dubi, Gómez, & Schuller**, 2009), where individual switching mechanisms cannot be resolved. As device length reduces to 100 μm (Fig. 1b), negative differential resistance (NDR) emerges, indicating the onset of current-controlled switching dynamics characteristic of MIT materials (**Sharoni, Ramírez, & Schuller**, 2008).

Upon further miniaturization to 10 μm (Fig. 1c), the I-V characteristic transforms dramatically, displaying multiple sharp, discrete voltage jumps. These discrete events represent the emergence of distinct switching branches—clear evidence that multiple mechanisms with different characteristics operate simultaneously within the same device. The discrete switching events we observe are characteristic of devices in the 1-10 μm range, where individual domain switching can be resolved while maintaining sufficient current uniformity. In smaller devices (~100 nm), switching often occurs as a single jump due to the device dimensions approaching the typical VO_2 domain size (**Budai et al.**, 2014; **Fan et al.**, 2016), resulting in avalanche-like transitions. This evolution from continuous to discrete switching behavior demonstrates that our intermediate size range provides the optimal window for mechanism deconvolution by balancing domain resolution with measurement reproducibility, while device miniaturization enables resolution of individual switching pathways that coexist but are averaged out in larger geometries (**Zhong, Zhang, Gupta, & LeClair**, 2011).

Temperature-Dependent Switching Branch Identification

To deconvolute the nature of the different switching mechanisms, we performed comprehensive temperature-dependent measurements across the transition region. Figure 2a shows I-V curves measured across temperatures from 294 K to 335 K, spanning the bulk MIT temperature of VO_2. The systematic evolution with temperature provides crucial information about the underlying physics: if all switching events were driven by the same mechanism, they would exhibit uniform temperature dependencies.

Instead, we observe complex, non-uniform changes that suggest multiple mechanisms responding differently to thermal activation. Figure 2b provides magnified views of the discrete voltage jumps and their varied temperature evolution. Importantly, different jumps exhibit markedly different responses to temperature changes—some shift significantly with temperature while others remain relatively stable, providing direct evidence for the coexistence of distinct physical mechanisms.

By calculating the numerical derivative dV/dI (Fig. 2c), we precisely locate switching events and generate the comprehensive map shown in Figure 2d. This analysis reveals well-defined switching branches (A0, A1, A2, A3), each representing a distinct pathway with its own characteristic temperature dependence. The structured nature of this map demonstrates that the apparent complexity of VO_2 switching arises from the superposition of multiple, individually well-behaved mechanisms rather than from chaotic or random processes.

The systematic appearance of well-defined branches across all device geometries (Figs. 2, 3), each showing characteristic temperature dependencies reproducible over $>$50 I-V sweeps per device, confirms that these represent intrinsic VO_2 mechanisms rather than device-specific artifacts. Bulk characterization via XRD and transport verified that all films exhibit the canonical MIT at $T_{MIT} \sim 340$ K, validating intrinsic material properties.

Quantitative Deconvolution of Electronic and Thermal Mechanisms

The switching branch map enables clear deconvolution of the coexisting mechanisms based on their fundamental temperature dependencies, providing direct experimental access to the orbital-selective transition picture proposed by recent theoretical work (**Kim et al.**, 2022; **Budai et al.**, 2014).

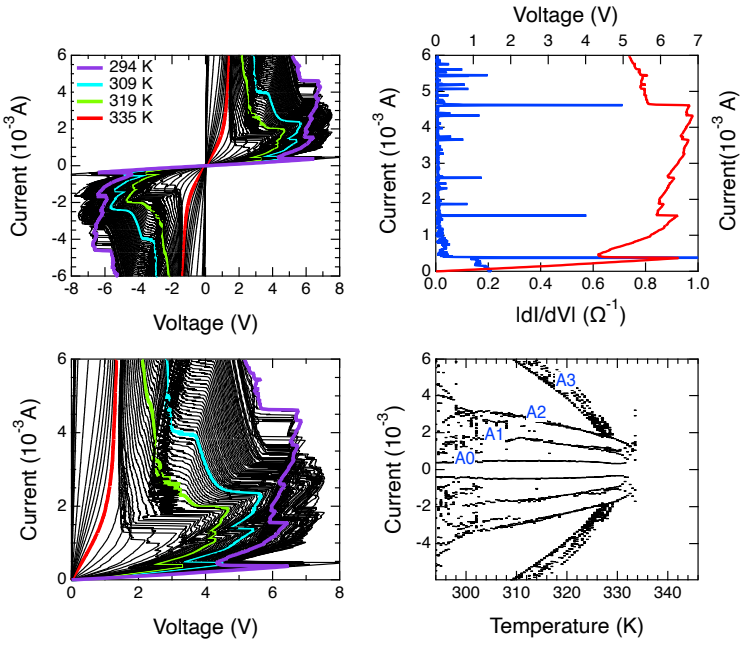

Figure 2. Temperature-dependent switching mechanism identification. (a) Complete I-V curves across temperature range showing systematic evolution of switching thresholds. (b) Magnified view revealing differential temperature-dependent dynamics of voltage jumps. (c) dV/dI derivative analysis for precise switching event identification. (d) Switching mechanism map revealing distinct branches (A0, A1, A2, A3) corresponding to different physical pathways, establishing the experimental foundation for mechanism deconvolution. Z1, Z2 and Z3 regions in d identify temperature ranges at which a mix of thermal and non-thermal branches appear (Z1), strong thermal branches (Z2) and no branches at al (Z3) appears

Electronic-Dominated Branches: Branches A0 and A1 are identified as electronic-dominated due to their weak temperature dependence, maintaining relatively constant critical currents across the measured temperature range. This behavior is the hallmark of a non-thermal switching mechanism. One compelling explanation, recently demonstrated in VO_2, is field-assisted carrier generation from in-gap defect states, which triggers a doping-driven MIT far below the thermal transition temperature (**Kalcheim et al.**, 2020). This interpretation is supported by studies on identically-fabricated samples characterizing disorder effects (**Ramírez et al.**, 2015), oxygen vacancy states (**Dietze et al.**, 2014), thermal heating's role (**Zimmers et al.**, 2013), and ultrafast dynamics (**Wang et al.**, 2017).

Other field-assisted m echanisms have also been proposed, including intrinsic Zener-type breakdown across the Mott gap (**Oka, Arita, & Aoki**, 2003; **Stefanovich, Pergament, & Stefanovich**, 2000) and direct field-induced destabilization of the correlated insulating state (**Stoliar et al.**, 2013). While our results do not exclude these other possibilities, the specific temperature and geometric dependencies observed in our devices are particularly well-described by the defect-mediated carrier generation model.

For instance, this mechanism is consistent with the observed geometric scaling. The critical electric field required for carrier emission from defects, $E_{c,\mathrm{elec}}$, is an intrinsic property. Given that the critical voltage scales with length ($V_c = E_c L$) and the device resistance also scales approximately with length ($R \propto L$), the resulting critical current ($I_c = V_c/R$) is expected to be largely independent of device size, in agreement with our findings for these branches.

Revista de la Academia Colombiana de Ciencias Exactas, Físicas y Naturales. 2026
doi: https://doi.org/10.18257/raccefyn.3273

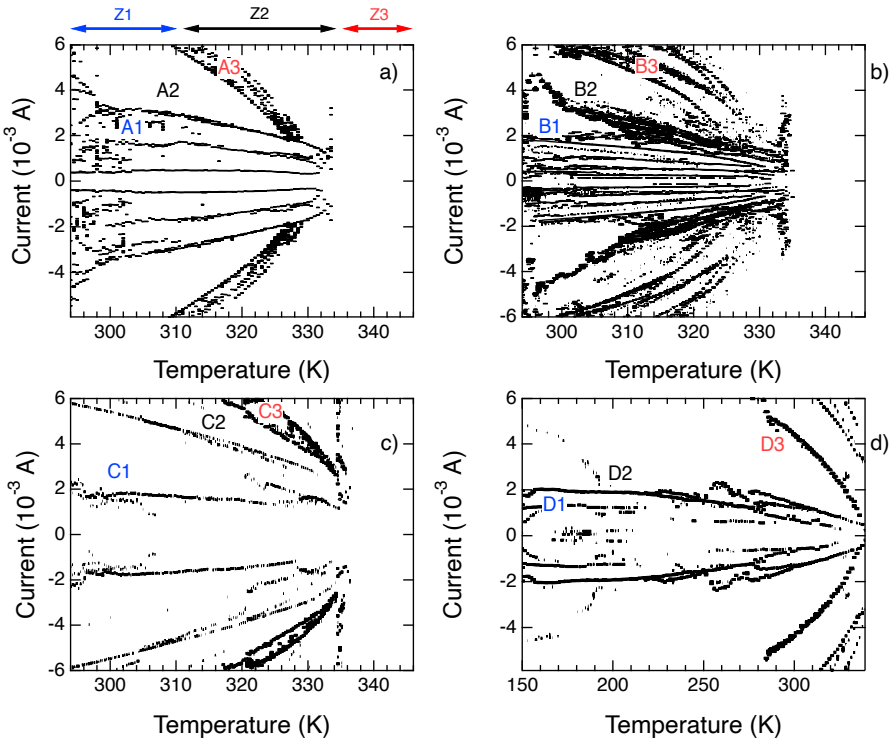

Figure 3. Geometric scaling of switching mechanism landscapes. Switching maps for devices of length (a) 1 μm, (b) 3 μm, (c) 5 μm, and (d) 10 μm. Smaller devices exhibit more numerous discrete switching branches, enabling enhanced resolution of individual mechanisms through reduced ensemble averaging effects. The reproducibility of branch patterns across geometries confirms intrinsic switching mechanisms.

Thermal-Dominated Branches: Branches A2 and A3 display strong, systematic temperature dependence, which is the hallmark of Joule heating-driven processes. As shown in Fig. 4, these branches follow a parabolic relationship where the critical power required for switching ($P_c = I_c^2 R$) decreases linearly as the ambient temperature (T_a) approaches the transition temperature (T_{MIT}). This behavior, well-described by $I_c^2 \propto (T_{\mathrm{MIT}} - T_{\mathrm{a}})$, is characteristic of processes where the applied current must heat a localized region of the device to a critical temperature, corresponding to the thermal (Peierls-like) component of the MIT. The geometric scaling of the critical current for these thermal branches reveals a more complex picture involving competing heat dissipation pathways, which is analyzed in detail in the following section.

The coexistence of these different branch types within a single device provides direct experimental validation for theoretical predictions of orbital-selective mechanisms operating simultaneously (**Tomczak & Biermann**, 2012; **Fan et al.**, 2016). Our methodology provides a robust and quantitative visualization of this fundamental coexistence, building on previous work that distinguished between thermal and non-thermal pathways. By mapping the critical switching currents across a wide parameter space, we can clearly separate and analyze the distinct branches corresponding to each mechanism.

Geometric Scaling and Mechanism Validation

Figure 3 presents switching maps for devices with L = 1, 3, 5, and 10 μm, revealing how the relative prominence of different mechanisms varies with device geometry. Smaller devices (1-3 μm) exhibit richer structure with numerous well-resolved branches, consistent with reduced ensemble averaging and enhanced sensitivity to individual mechanism contributions

(**Manca, Kanki, Tanaka, Marrè, & Pellegrino**, 2015; **Radu et al.**, 2015). Importantly, all device sizes show evidence of both thermal and electronic branches, confirming that both mechanisms are intrinsic to VO_2 switching behavior.

Further validation of the thermal mechanism is obtained from a quantitative analysis of the geometric scaling of the critical current, I_c. Figure 5 plots the critical current at 320 K, extracted from the primary thermal branches of the devices shown in Fig. 3 (blue circles); the error bars are estimated from the current range of each switching branch.

The data reveals that the dependence of I_c on device length L does not follow a simple power law. Specifically, the critical current decreases more slowly with increasing L than predicted by a model considering only 1D heat dissipation to the contacts ($I_c \propto L^{-1}$, black line). This deviation indicates the presence of a competing, length-independent heat loss mechanism, which we attribute to conduction into the substrate.

Consequently, the experimental data is well-described by a composite model that accounts for these two parallel dissipation channels, as detailed in the Appendix. The model, given by $I_c(L) = C_0 + C_1/L$, combines a constant term C_0 for substrate loss ($I_c \propto L^0$) with a term C_1/L for contact loss ($I_c \propto L^{-1}$). The agreement between this model and the data provides confirmation of the thermal nature of these switching branches. While our analytical model captures the general physics of the geometric scaling, a more detailed numerical treatment could provide further refinement. For instance, resistor network models that explicitly include inter-domain thermal coupling during phase coexistence have successfully described complex switching phenomena in similar devices (**Guénon et al.**, 2013).

Temporal Dynamics and Volatile Switching Characteristics

Similarly as in the IV measurements, we employed the delta current-reversal technique to characterize the dynamics of the switching events shown in Fig. 2. Following the initial pulsed I-V characterization to identify switching thresholds, we selected specific current values to apply controlled pulse trains and captured the real-time voltage response using an oscilloscope with microsecond temporal resolution.

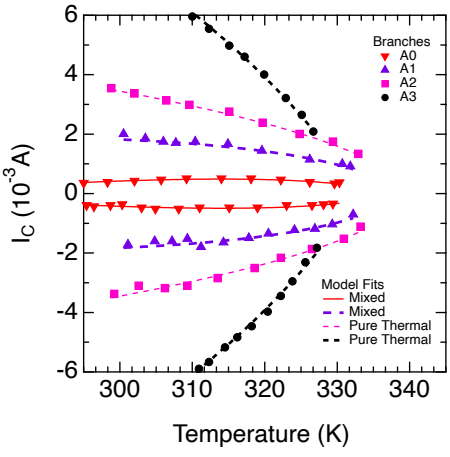

Figure 4. Quantitative validation of dual switching mechanisms. Experimental data (symbols) fitted with theoretical models (lines). Electronic-dominated branches (A0, A1) show weak temperature dependence consistent with field-driven mechanisms. Thermal branches (A2, A3) exhibit a pure parabolic dependence ($I_c^2 \propto (T_{\mathrm{MIT}} - T_a)$) characteristic of Joule heating processes. Excellent agreement validates the mechanism deconvolution approach.

Revista de la Academia Colombiana de Ciencias Exactas, Físicas y Naturales. 2026
doi: https://doi.org/10.18257/raccefyn.3273

The temporal dynamics of the switching process are shown in Fig. 6 for a 1 μm device. The pulsed I-V characteristic in Fig. 6(a) displays negligible hysteresis, indicating that cumulative heating effects are minimized. Below the switching threshold (at 0.50 and 1.50 mA), the voltage response is linear and resistor-like (Fig. 6b). In contrast, when the current exceeds the threshold (at 3.70 and 6.00 mA), the device response changes dramatically. The onset of the current pulse induces a large, transient voltage spike that quickly relaxes to a stable, low-resistance metallic state, as shown in Fig. 6c-e. This behavior reflects the complex, non-equilibrium process of metallic filament nucleation, which is governed by the interplay between fast electronic switching and slower, microsecond-scale thermal equilibration (**Grandi et al.**, 2020).

The recovery after current removal reveals a two-stage relaxation process. A rapid voltage drop within tens of microseconds indicates an avalanche-like collapse of the percolative metallic network, followed by a slower exponential decay on the order of hundreds of microseconds, reflecting thermal dissipation and structural relaxation back to the insulating phase (for instance, refer to Fig. 6d at 260 μs).

Discussion

Our experimental deconvolution of switching mechanisms provides direct support for the modern understanding of the VO_2 MIT as a cooperative phenomenon. The traditional picture of competing thermal versus electronic mechanisms is revealed as an oversimplification. Instead, our results visualize a landscape where both mechanisms coexist and operate simultaneously.

The temperature-independent branches represent the electronic (Mott-like) aspect of the transition (**Kim et al.**, 2022; **Qazilbash et al.**, 2007), aligning with ultrafast studies showing sub-picosecond electronic switching that precedes structural changes (**Wall et al.**, 2018; **Pashkin et al.**, 2011). The parabolic thermal branches represent the structural (Peierls-like) aspect, where Joule heating provides the energy for lattice distortion (**Budai et al.**, 2014; **Cocker et al.**, 2012).

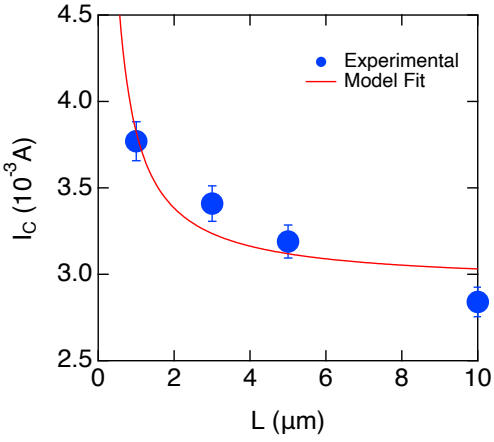

Figure 5. The critical current (I_c) for the thermal branches is plotted as a function of device length (L) at T = 320 K. The data is fit to a composite thermal model (red line), Eq. 13, that accounts for two competing heat dissipation pathways: (1) a length-independent contribution from heat loss to the substrate ($I_c \propto L^0$, green line), and (2) a length-dependent contribution from 1D heat conduction to the contacts ($I_c \propto L^{-1}$, black line). See Appendix for details on the model.

The distinct temperature dependencies we observe likely reflect different stages and types of switching events. The temperature-independent electronic branches (A0, A1) are consistent with a non-thermal switching mechanism driven by field-assisted carrier generation from in-gap defect states, as recently demonstrated in VO_2 nanowires (**Kalcheim et al.**, 2020). In this scenario, the electric field lowers the energy barrier for exciting trapped carriers, leading to a doping-driven destabilization of the insulating state that occurs far below the thermal T_{MIT}. This mechanism provides a clear physical basis for the weak temperature dependence we observe. Furthermore, the existence of multiple, distinct electronic branches in our data (A0, A1) can be interpreted as the activation of different families of defect sites, each with a unique threshold field for carrier emission, or avalanche-like percolation processes.

In contrast, the thermal branches (A2, A3) represent the subsequent, more global switching of the device, where Joule heating provides the energy for lattice distortion and V-V dimer formation, consistent with the classic Peierls-like aspect of the transition (**Budai et al.**, 2014; **Cocker et al.**, 2012). Our work thus visualizes the coexistence of these non-thermal nucleation events and subsequent thermally-driven domain expansion within a single device.

This study connects the fundamental physics of MITs with a practical characterization methodology. The technique operates under realistic device conditions, provides quantitative separation of mechanisms, and scales across different device geometries. This approach could be extended to other correlated oxides where similar mechanism competition exists, such as V_2O_3, NbO_2, and the nickelate family (**del Valle et al.**, 2018).

It is important to note our temporal resolution ($\sim \mu$s) cannot distinguish ultrafast processes (fs-ps Mott dynamics vs. ns thermal effects), though prior pump-probe studies on identical samples (**Wang et al.**, 2017) showed thermal effects at ps-ns and Mott processes at fs timescales. The electronic branches may include contributions from defect-mediated carrier injection (**Dietze et al.**, 2014; **Ramírez et al.**, 2015) in addition to intrinsic field effects. However, the systematic geometric scaling supports significant intrinsic contributions. The fundamental role of thermal heating established previously (**Zimmers et al.**, 2013) motivates our pulsed approach to isolate non-thermal pathways.

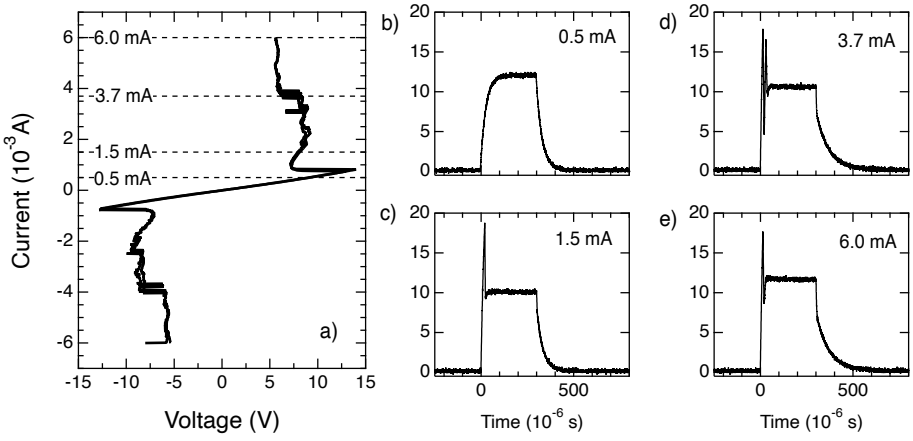

Figure 6. Temporal dynamics revealing electronic-thermal mechanism interplay. (a) I-V characteristic showing discrete switching levels. (b-e) Time-dependent voltage response to current pulses at different levels (0.50, 1.50, 3.70, and 6.00 mA). Transient voltage spikes at higher currents reveal the complex interplay between rapid electronic switching and slower thermal processes during domain formation and relaxation.

Revista de la Academia Colombiana de Ciencias Exactas, Físicas y Naturales. 2026
doi: https://doi.org/10.18257/raccefyn.3273

From a practical standpoint, the ability to identify and control specific s witching pathways enables rational device design. Electronic branches provide fast, temperature-stable switching suitable for high-speed applications, while thermal branches offer slower, history-dependent dynamics useful for adaptive memory elements. Similar controls have also been reported (**Del Valle, Ramírez, Rozenberg, & Schuller**, 2019) in VO_2, validating our method. Furthermore, the geometric scaling analysis, revealing a crossover from an L^{-1} dependence for short devices to a length-independent behavior for long devices, provides a more sophisticated design rule for predicting and controlling power consumption in thermally-activated devices, while the size-independent electronic branches offer scaling advantages for high-density applications.

Conclusion

We have developed and demonstrated a comprehensive temperature-dependent methodology that successfully deconvolutes the coexisting thermal and electronic switching mechanisms in VO_2 devices. Our results provide direct experimental evidence for the cooperative nature of the metal-insulator transition, showing that the complex switching landscape represents a superposition of distinct, well-defined e lectronic (athermal) a nd t hermal (Joule heating-driven) branches.

This work provides a powerful framework for interpreting the cooperative nature of the VO_2 MIT. The thermal branches, driven by Joule heating, can be clearly associated with the structural (Peierls-like) aspects of the transition. The electronic branches, while definitively non-thermal, could originate from several field-driven phenomena, including intrinsic effects on the correlated electron system or extrinsic, defect-mediated processes. While our methodology cannot distinguish between these microscopic origins, it provides the essential experimental separation needed to test and refine theories that connect these macroscopic pathways to the underlying Mott and Peierls physics. It thus offers a new tool to probe the interplay between electronic and structural degrees of freedom in correlated systems.

Our findings demonstrate that the rich dynamics of VO_2 switching results from the interaction between different physical mechanisms. The de-convolution of the switching landscape into separate electronic and thermal branches provides a clear map of these pathways. Furthermore, the temporal dynamics reveal their real-time cooperation, showing fast, avalanche-like electronic nucleation events followed by slower thermal relaxation processes. This understanding allows for opportunities for device design that can harness the full cooperative nature of the metal-insulator transition.

Acknowledgments

I am deeply grateful to the many individuals and institutions who have contributed to my scientific journey and this research. I extend my heartfelt thanks to my PhD advisors, Maria Elena Gomez at Universidad del Valle and Ivan K. Schuller at UC San Diego, whose guidance and mentorship were instrumental throughout my research. Also, I extend my gratitude to Dr. Amos Sharoni, from which I learn many things and who also contribute to the sample preparation of the samples reported here.

I am especially grateful to Professor Gomez, who has supported and taught me since my undergraduate studies; her invaluable help has been crucial to my success in my scientific career. I am equally thankful to Professor Schuller for his invaluable teachings and for welcoming me as a postdoc in his laboratory. I also wish to acknowledge Pedro Prieto, Professor at Universidad del Valle and long-time director of the Thin Film Laboratory, from whom I learned immensely, both within academia and beyond.

I appreciate fruitful discussions with Dr. Ali Basaran and Dr. Pavel Salev, who greatly enrich this manuscript.

I acknowledge financial support from Facultad de Ciencias (INV-2025-213-3450) and Vicerrectoría de Investigaciones of Universidad de los Andes, Bogotá, Colombia, and Colciencias/Minciencias. I thank the international collaborations with University of California San Diego. I am grateful to colleagues from Colombia and abroad who contributed to the results referenced in this work.

Author Contributions

JGR: Conceptualization, investigation, data analysis, original draft writing.

Conflict of Interest

The authors declare they have no known competing financial interests or personal relationships that could have appeared to influence the work reported in this paper.

Appendix

Thermal Scaling Models for Joule Heating

The geometric scaling of the critical current (I_c) for thermally driven switching can be understood by analyzing the steady-state solutions to the general heat diffusion equation:

$$\frac{\partial T}{\partial t} = \alpha \nabla^2 T + \frac{J^2 \rho}{\rho_{mass} C_p} - k(T - T_0), \tag{1}$$

where T is the local temperature, t is time, α is the thermal diffusivity, J is the current density, ρ is the electrical resistivity, ρ_{mass} is the mass density, C_p is the specific heat capacity, k is an effective heat transfer coefficient representing loss to the substrate, and T_0 is the ambient substrate temperature.

In steady state ($\partial T/\partial t = 0$), this equation describes the balance between heat generation (Joule heating) and heat dissipation. The following models explore two primary, competing heat dissipation channels derived as limiting cases of this equation.

Model 1: 1D Heat Conduction to Contacts

This model assumes that the primary mechanism for heat removal is conduction along the length of the conductive filament to the large metallic electrodes, which act as heat sinks at the ambient temperature (T_a). This pathway is most dominant in short devices or those on thermally insulating substrates.

In steady state, the total power generated by Joule heating (P_{gen}) must equal the power removed by thermal conduction (P_{cond}). The generated power is given by:

$$P_{gen} = I_c^2 R = I_c^2 \frac{\rho L}{A_{eff}} \tag{2}$$

where R is the resistance of the filament, ρ is its resistivity, L is its length, and A_{eff} is its effective cross-sectional area.

The heat conducted away is governed by the temperature difference between the filament's center (at the transition temperature, T_{MIT}) and the contacts (at T_a), and the thermal resistance of the filament (R_{th}):

$$P_{cond} = \frac{T_{MIT} - T_a}{R_{th}} \tag{3}$$

Revista de la Academia Colombiana de Ciencias Exactas, Físicas y Naturales. 2026
doi: https://doi.org/10.18257/raccefyn.3273

For 1D conduction along the filament, the thermal resistance is:

$$R_{th} = \frac{L}{\kappa A_{eff}} \tag{4}$$

where κ is the thermal conductivity of the filament material.

By equating the generated and conducted power at the critical threshold ($P_{gen} = P_{cond}$), we can solve for the critical current I_c:

$$I_c^2 \frac{\rho L}{A_{eff}} = \frac{T_{MIT} - T_a}{L/(\kappa A_{eff})} \tag{5}$$

Rearranging for I_c^2 yields:

$$I_c^2 = \frac{\kappa A_{eff}^2 (T_{MIT} - T_a)}{\rho} \frac{1}{L^2} \tag{6}$$

This leads to a scaling relationship where the critical current is inversely proportional to the device length:

$$I_c \propto \frac{1}{L} \quad \text{or} \quad I_c \propto L^{-1} \tag{7}$$

Model 2: Heat Conduction to Substrate

This model assumes that the dominant heat dissipation pathway is perpendicular to the current flow, down into the thermally conductive substrate. This mechanism becomes increasingly important for longer devices where the thermal resistance to the contacts is high.

Here, we consider the heat balance per unit length of the filament. The heat generated per unit length (p_{gen}) is:

$$p_{gen} = I_c^2 \frac{R}{L} = I_c^2 \frac{\rho}{A_{eff}} \tag{8}$$

This heat is lost to the substrate with a thermal resistance per unit length, r_{th}. The value of r_{th} depends on the geometry of the interface and the thermal properties of the substrate, but it is independent of the device length L. The heat lost per unit length (p_{loss}) is:

$$p_{loss} = \frac{T_{MIT} - T_a}{r_{th}} \tag{9}$$

Equating the heat generation and loss per unit length at the threshold ($p_{gen} = p_{loss}$):

$$I_c^2 \frac{\rho}{A_{eff}} = \frac{T_{MIT} - T_a}{r_{th}} \tag{10}$$

Solving for I_c^2 gives:

$$I_c^2 = \frac{A_{eff}(T_{MIT} - T_a)}{\rho r_{th}} \tag{11}$$

Since all terms on the right-hand side of this equation are independent of the device length L, this model predicts that the critical current is also independent of length:

$$I_c \propto L^0 \tag{12}$$

Combined Model for Competing Pathways

In a realistic device, both heat dissipation pathways operate in parallel. The total heat loss is the sum of the loss to the contacts and the loss to the substrate. The observed scaling

behavior can be understood as a crossover between these two regimes. A composite model can be constructed by summing the contributions of the two mechanisms. The total critical current can be modeled as:

$$I_c(L) = I_{substrate} + I_{electrode}(L) = C_0 + \frac{C_1}{L} \tag{13}$$

where C_0 is a constant representing the length-independent contribution from substrate heat loss, and C_1/L represents the length-dependent contribution from heat loss to the electrodes. This combined model accurately describes the experimental data across all measured device lengths, capturing the transition from a regime dominated by conduction to the contacts (for short L) to one dominated by conduction to the substrate (for long L).

Referencias

Budai, J. D., Hong, J., Manley, M. E., Specht, E. D., Li, C. W., Tischler, J. Z., Abernathy, D. L., Said, A. H., Leu, B. M., Boatner, L. A., McQueeney, R. J., & Delaire, O. (2014). Metallization of vanadium dioxide driven by large phonon entropy. *Nature*, *515*(7528), 535-539. https://doi.org/10.1038/nature13865

Chen, S., Wang, Z., Ren, H., Chen, Y., Yan, W., Wang, C., Li, B., Jiang, J., & Zou, C. (2019). Gate-controlled VO_2 phase transition for high-performance smart windows. *Science Advances*, *5*(3), Article eaav6815. https://doi.org/10.1126/sciadv.aav6815

Cocker, T. L., Titova, L. V., Fourmaux, S., Holloway, G., Bandulet, H.-C., Brassard, D., Kieffer, J.-C., El Khakani, M. A., & Hegmann, F. A. (2012). Phase diagram of the ultrafast photoinduced insulator-metal transition in vanadium dioxide. *Physical Review B*, *85*(15), Article 155120. https://link.aps.org/doi/10.1103/PhysRevB.85.155120

Crunteanu, A., Givernaud, J., Leroy, J., Mardivirin, D., Champeaux, C., Orlianges, J.-C., Catherinot, A., & Blondy, P. (2010). Voltage- and current- activated metal-insulator transition in VO_2-based electrical switches: a lifetime operation analysis. *Science and Technology of Advanced Materials, 11*(6), Article 065002. https://doi.org/10.1088/1468-6996/11/6/065002

Del Valle, J., Pavel, S., Tesler, F., Vargas, N. M., Kalcheim, Y., Wang, P., Trastoy, J., Lee, M.-H., Kassabian, G., Ramírez, J. G., Rozenberg, M. J., & Schuller, I. K. (2019). Subthreshold firing in Mott nanodevices. *Nature, 569*(7756), 388-392. https://doi.org/10.1038/s41586-019-1159-6

Del Valle, J., Ramírez, J. G., Rozenberg, M. J., & Schuller, I. K. (2018). Challenges in materials and devices for resistive-switching-based neuromorphic computing. *Journal of Applied Physics*, *124*(21), 211101. https://doi.org/10.1063/1.5047800

Dietze, S. H., Marsh, M. J., Wang, S., Ramírez, J.-G., Cai, Z.-H., Mohanty, J. R., Schuller, I. K., & Shpyrko, O. G. (2014). X-ray-induced persistent photoconductivity in vanadium dioxide. *Physical Review B*, *90*(16), 165109. https://doi.org/10.1103/PhysRevB.90.165109

Guénon, S., Scharinger, S., Wang, S., Ramírez, J. G., Koelle, D., Kleiner, R., & Schuller, I. K. (2013). Electrical breakdown in a V_2O_3 device at the insulator-to-metal transition. *Europhysics Letters, 101*(5), 57003. https://doi.org/10.1209/0295-5075/101/57003

Jager, M. F., Ott, C., Kraus, P. M., Kaplan, C. J., Pouse, W., Marvel, R. E., Haglund, R. F., Neumark, D. M., & Leone, S. R. (2017). Tracking the insulator-to-metal phase transition in VO_2 with few-femtosecond extreme UV transient absorption spectroscopy. *Proceedings of the National Academy of Sciences*, *114*(36), 9558-9563. https://doi.org/10.1073/pnas.1707602114

Joushaghani, A., Jeong, J., Paradis, S., Alain, D., Aitchison, J. S., & Poon, J. K. S. (2015). Wavelength-size hybrid Si-VO_2 waveguide electroabsorption optical switches and photodetectors. *Optics Express, 23*(3), 3657-3668. https://doi.org/10.1364/OE.23.003657

Kalcheim, Y., Camjayi, A., del Valle, J., Salev, P., Rozenberg, M., & Schuller, I. K. (2020). Non-thermal resistive switching in Mott insulator nanowires. *Nature Communications, 11*(1), 2985. https://doi.org/10.1038/s41467-020-16752-1

Kim, S., Backes, S., Yoon, H., Kim, W., Sohn, C., Son, J., Biermann, S., Noh, T. W., & Park, S. Y. (2022). Orbital-selective Mott and Peierls transition in H_xVO_2. npj *Quantum Materials, 7*(95), 2397-4648. https://doi.org/10.1038/s41535-022-00505-y

Revista de la Academia Colombiana de Ciencias Exactas, Físicas y Naturales. 2026
doi: https://doi.org/10.18257/raccefyn.3273

Li, D., Sharma, A. A., Gala, D. K., Shukla, N., Paik, H., Datta, S., Schlom, D. G., Bain, J. A., & Skowronski, M. (2016). Joule Heating-Induced Metal–Insulator Transition in Epitaxial VO_2/TiO_2. *ACS Applied Materials & Interfaces, 8*(26), 12908-12914. https://doi.org/10.1021/acsami.6b03501

Manca, N., Kanki, T., Tanaka, H., Marré, D., & Pellegrino, L. (2015). Influence of thermal boundary conditions on the current-driven resistive transition in VO_2 microbridges. *Applied Physics Letters, 107*(14), Article 143508. https://doi.org/10.1063/1.4933014

Markov, P., Marvel, R. E., Conley, H. J., Miller, K. J., Haglund, R. F. J., & Weiss, S. M. (2015). Optically monitored electrical switching in VO_2. *ACS Photonics, 2*(8), 1175-1182. https://doi.org/10.1021/acsphotonics.5b00244

Morrison, V. R., Chatelain, R. P., Tiwari, K. L., Hendaoui, A., Bruhács, A., Chaker, M., & Siwick, B. J. (2014). A photoinduced metal-like phase of monoclinic VO_2 revealed by ultrafast electron diffraction. *Science, 346*(6208), 445-448. https://doi.org/10.1126/science.1253779

Murtagh, O., Walls, B., & Shvets, I. V. (2020). Controlling the resistive switching hysteresis in VO_2 thin films via application of pulsed voltage. *Applied Physics Letters, 117*(6), Article 063501. https://doi.org/10.1063/5.0017784

O'Callahan, B. T., Jones, A. C., Hyung Park, J., Cobden, D. H., Atkin, J. M., & Raschke, M. B. (2015). Inhomogeneity of the ultrafast insulator-to-metal transition dynamics of VO_2. *Nature Communications, 6*(1), Article 6849. https://doi.org/10.1038/ncomms7849

Oka, T., Arita, R., & Aoki, H. (2003). Breakdown of a Mott insulator: A nonadiabatic tunneling mechanism. *Physical Review Letters, 91*(6), Article 066406. https://doi.org/10.1103/PhysRevLett.91.066406

Pashkin, A., Kübler, C., Ehrke, H., Lopez, R., Halabica, A., Haglund Jr., R. F., Huber, R., & Leitenstorfer, A. (2011). Ultrafast insulator-metal phase transition in VO_2 studied by multiterahertz spectroscopy. *Physical Review B, 83*(19), Article 195120. https://doi.org/10.1103/PhysRevB.83.195120

Pósa, L., Hornung, P., Török, T. N., Schmid, S. W., Arjmandabasi, S., Molnár, G., Baji, Z., Dražić, G., Halbritter, & A., Volk, J. Halbritter, A. E., & Volk, J. (2023). Interplay of Thermal and Electronic Effects in the Mott Transition of Nanosized VO_2 Phase Change Memory Devices. *ACS Applied Nano Materials, 6*(11), 9137- 9147. https://doi.org/10.1021/acsanm.3c00150

Pouget, J. P., Launois, H., D'Haenens, J. P., Merenda, P., & Rice, T. M. (1975). Electron localization induced by uniaxial stress in pure VO_2. *Physical Review Letters, 35*(13), 873-875. https://doi.org/10.1103/PhysRevLett.35.873

Qazilbash, M. M., Brehm, M., Chae, B.-G., Ho, P.-C., Andreev, G. O., Kim, B.-J., Yun, S. J., Balatsky, A. V., Maple, M. B., Keilmann, F., Kim, H.-T., & Basov, D. N. (2007). Mott transition in VO_2 revealed by infrared spectroscopy and nano-imaging. *Science, 318*(5857), 1750-1753. https://doi.org/10.1126/science.1150124

Radu, I. P., Govoreanu, B., Mertens, S., Shi, X., Cantoro, M., Schaekers, M., Jurczak, M., De Gendt, S., Stesmans, A., Kittl, J. A., Heyns, M., & Martens, K. (2015). Switching mechanism in two-terminal vanadium dioxide devices. *Nanotechnology, 26*(16), Article 015201. https://doi.org/10.1088/0957-4484/26/16/165202

Ramírez, J. G., Saerbeck, T., Wang, S., Trastoy, J., Malnou, M., Lesueur, J., Crocombette, J. P., Villegas, J. E., & Schuller, I. K. (2015). Effect of disorder on the metal-insulator transition of vanadium oxides: Local versus global effects. *Physical Review B, 91*(20), Article 205123. https://doi.org/10.1103/PhysRevB.91.205123

Ramírez, J.-G., Sharoni, A., Dubi, Y., Gómez, M. E., & Schuller, I. K. (2009). First-order reversal curve measurements of the metal-insulator transition in VO_2: Signatures of persistent metallic domains. *Physical Review B, 79*(23), Article 235110. https://link.aps.org/doi/10.1103/PhysRevB.79.235110

Rana, A., Li, C., Koster, G., & Hilgenkamp, H. (2020). Resistive switching studies in VO_2 thin films. *Scientific Reports, 10*(1), 3293. https://doi.org/10.1038/s41598-020-60373-z

Rathi, S., Park, J. H., Lee, I. -Y., Baik, J. M., Yi, K. S., & Kim, G.-H. (2014). Unravelling the switching mechanisms in electric field induced insulator-metal transitions in VO_2 nanobeams. *Journal of Physics D: Applied Physics*, *47*(29), Article 295101. https://doi.org/10.1088/0022-3727/47/29/295101

Sharoni, A., Ramírez, J. G., & Schuller, I. K. (2008). Multiple Avalanches across the Metal-Insulator Transition of Vanadium Oxide Nanoscaled Junctions. *Physical Review Letters, 101*(2), Article 026404. https://link.aps.org/doi/10.1103/PhysRevLett.101.026404

Shukla, N., Parihar, A., Freeman, E., Paik, H., Stone, G., Narayanan, V., Wen, H., Cai, Z., Gopalan, V., Engel-Herbert, R., Schlom, D. G., Raychowdhury, A., & Datta, S. (2014). Synchronized charge oscillations in correlated electron systems. *Scientific Reports, 4*(1), Article 4964. https://doi.org/10.1038/srep04964

Sood, A., Shen, X., Shi, Y., Kumar, S., Park, S. J., Zajac, M., Sun, Y., Chen, L.-Q., Ramanathan, S., Wang, X., Chueh, W. C., & Lindenberg, A. M. (2021). Universal phase dynamics in VO_2 switches revealed by ultrafast operando diffraction. *Science, 373*(6551), 352–355. https://doi.org/10.1126/science.abc0652

Stefanovich, G., Pergament, A., & Stefanovich, D. (2000). Electrical switching and Mott transition in VO_2. *Journal of Physics: Condensed Matter, 12*(41), Article 8837. https://doi.org/10.1088/0953-8984/12/41/310

Stoliar, P., Cario, L., Janod, E., Corraze, B., Guillot-Deudon, C., Salmon-Bourmand, S., Guiot, V., Tranchant, J., & Rozenberg, M. (2013). Universal electric-field-driven resistive transition in narrow-gap mott insulators. *Advanced Materials, 25*(23), 3222–3226. https://doi.org/10.1002/adma.201301113

Valmianski, I., Wang, P. Y., Wang, S., Ramírez, J. G., Guénon, S., & Schuller, I. K. (2018). Origin of the current-driven breakdown in vanadium oxides: Thermal versus electronic. *Physical Review B, 98*(19), Articles 195144. https://doi.org/10.1103/PhysRevB.98.195144

Wang, S., Ramírez, J. G., Jeffet, J., Bar-Ad, S., Huppert, D., & Schuller, I. K. (2017). Ultrafast photo-induced dynamics across the metal-insulator transition of VO_2. *Europhysics Letters, 118*(2), Article 27005. https://doi.org/10.1209/0295-5075/118/27005

Weber, C., O'Regan, D. D., Hine, N. D. N., Payne, M. C., Kotliar, G., Littlewood, & P. B. (2012). Vanadium dioxide: A Peierls-Mott insulator stable against disorder. *Physical Review Letters, 108*(25), Article 256402. https://link.aps.org/doi/10.1103/PhysRevLett.108.256402

Yang, M., Yang, Y., Hong, B., Wang, L., Hu, K., Dong, Y., Xu, H., Huang, H., Zhao, J., Chen, H., Song, L. Ju, H., Zhu, J., Bao, J., Li, X., Gu, Y., Yang, T., Gao, X., Luo, Z., & Gao, C. (2016). Suppression of structural phase transition in VO_2 by epitaxial strain in vicinity of Metal-insulator Transition. Scientific Reports, *6*(1), 23119. https://doi.org/10.1038/srep23119

Zhong, X., Zhang, X., Gupta, A., & LeClair, P. (2011). Avalanche breakdown in microscale VO_2 structures. *Journal of Applied Physics, 110*(8), Article 084516. https://doi.org/10.1063/1.3654121

Zimmers, A., Aigouy, L., Mortier, M., Sharoni, A., Wang, S., West, K. G., Ramirez, J. G., & Schuller, I. K. (2013). Role of thermal heating on the voltage induced insulator-metal transition in VO_2. *Physical Review Letters, 110*(5), Article 056601. https://doi.org/10.1103/PhysRevLett.110.056601